Available online at www.sciencedirect.com
SCIENCE DIRECT®
Composites Science and Technology 63 (2003) 1581–1590
COMPOSITES SCIENCE AND TECHNOLOGY
www.elsevier.com/locate/compscitech

2-D nano-scale finite element analysis of a polymer field

Youqi Wang[a,*], Changjie Sun[a], Xuekun Sun[a], Jeffrey Hinkley[b], Gregory M. Odegard[b], Thomas S. Gates[b]

[a]Department of Mechanical and Nuclear Engineering, Kansas State University, Manhattan, KS 66506, USA
[b]NASA Langley Research Center, Hampton, VA 23681, USA

Received 23 September 2002; received in revised form 2 November 2002; accepted 15 December 2002

Abstract

Two types of 2-D nano-scale finite elements, the chemical bond element and the Lennard–Jones element, are formulated based upon inter-atomic and inter-molecular force fields. A nano-scale finite element method is employed to simulate polymer field deformation. This numerical procedure includes three steps. First, a polymer field is created by an off-lattice random walk, followed by a force relaxation process. Then, a finite element mesh is generated for the polymer field. Chemical bonds are modeled by chemical bond elements. If the distance between two non-bonded atoms or monomers is shorter than the action range of the Lennard–Jones attraction (or repulsion), a Lennard–Jones element is inserted between them. Finally, external load and boundary conditions are applied and polymer chain deformation is simulated step by step. During polymer deformation, failed Lennard–Jones bond elements are removed and newly formed Lennard–Jones elements are inserted into the polymer field during each loading step. The process continues until failure occurs. Two examples are presented to demonstrate the process. Stress–strain curves of polymer fields under unidirectional tensile load are derived. Continuum mechanical properties, such as modulus and polymer strength, are determined based upon the stress strain curve. Further, throughout the deformation process one observes polymer chain migration, nano-scale void generation, void coalescence and crack development.

Keywords: A. Polymer; Finite element analysis; Molecular mechanics; Nano-scale analysis

1. Introduction

Molecular dynamics is perhaps the most popular method currently employed for nano-scale analysis [1–9]. It has been employed to calculate polymer [1–3], nanotube [4–7] and nanotube reinforced polymer [8,9] modulus and strength. Using molecular dynamics, temperature induced high frequency molecular thermal vibration and static deformation can be simulated simultaneously. However, the frequency of molecular thermal vibration is on a scale of 10^{15} Hz. Consequently, molecular dynamics simulation can only provide deformations that occur on the too rapid scale of pico- or nano-seconds. As a result, the corresponding strain rate is much higher than found in typical engineering practice.

Monte Carlo simulation is another method that has been employed to investigate nano-scale polymer deformation [10–12]. The method is based upon statistical mechanics. Deformation is applied to the material domain via a series of strain increments accompanied by a series of Metropolis minimization cycles. Stress is expressed as a function of both potential energy and temperature. In practice, each strain increment step involves up to several hundred Metropolis energy minimization cycles. A typical example was presented by Chui and Boyce [11]. They simulated the deformation of amorphous polymers using the Monte-Carlo approach. Since the convergence of the process was slow, they could only obtain deformation information within a brief time scale. Strain rates used in their analyses ranged from 10^8 to 10^9/s, rates still similar to molecular dynamics.

For most engineering applications, material moduli remain approximately constant within a large temperature range. This means the high frequency of thermal

* Corresponding author. Tel.: +1-785-532-7181.
E-mail address: wang@mne.ksu.edu (Y. Wang).

0266-3538/03/$ - see front matter © 2003 Published by Elsevier Ltd.
doi:10.1016/S0266-3538(03)00068-X

dynamic molecular motion does not affect elastic deformation. Thus, a question arises: is it possible to decouple the elastic response of materials from the high frequency of thermal dynamical vibration in a molecular computational model?

In 1986, Theodorou and Suter [13] performed a detailed theoretical study of the contribution of molecular vibration to glassy polypropylene elastic constants. They concluded that only a negligible contribution to the modulus derives from high frequency molecular thermal vibration. They constructed an equilibrium atomic field for an amorphous polymer inside a cube. Each atom was assigned a small initial displacement based upon an iso-strain assumption. Because the assigned atomic field was not an equilibrium field, an energy minimization process was followed. Modulus was determined by derivatives of potential energy with respect to the strain component. This method saves a huge amount of computational time compared to either the Molecular Dynamics or the Monte Carlo approaches; however, it is of limited practical value: to determine the initial displacement of the atomic field for material domains of complex shape and complex load remains a difficult hurdle.

In this paper, a nano-scale finite element model is developed. First, nano-element stiffness matrices are formulated. The model is then used to simulate deformation and to calculate the stress–strain curve of the polymer field. Polymer chain migration and nano-scale void and crack creation are observed throughout the deformation of the polymer field.

This new approach allows decoupling of super high frequency thermal vibration from static molecular displacement in a molecular computational model. The high strain rate problem, unavoidable with molecular dynamical simulation, is thus eliminated. It provides efficiency similar to the method developed by Theodorou and Suter. Yet its usage is not restricted by material shape and loading complexity.

2. Formulation of two dimensional nano-scale elements

2.1. Atomic force field

The atomic force field is the core of molecular mechanics. It is derived from potential energy, which relates to deformation of chemical bonds and to intermolecular (e.g. Lennard–Jones) interaction.

2.2. Chemical bonds

The local geometry of chemical bonds of most materials can be characterized by a bond length r, bend angle θ and dihedral angle ϕ as shown in Fig. 1. Chemical bond deformation includes bond stretches (the change of bond length r), bond angle bends (the change of bond angle θ) and dihedral angle torsion (the change of dihedral angle ϕ). Additional terms are sometimes required to characterize local molecular structures and their deformations. A detailed discussion can be found in reference [14]. In a two-dimensional numerical model, only bond stretches and bond angle bends require discussion.

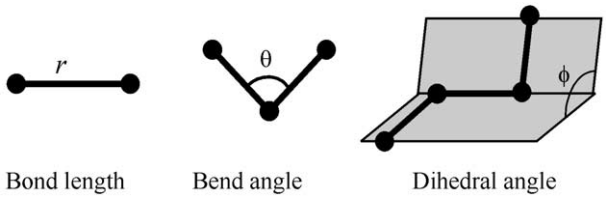

Fig. 1. Geometry of chemical bonds.

The simplest expression for potential energy that relates to bond stretch is the harmonic function [15–17]. It proposes a linear relationship between bond elongation (or shortening) and restoration force. The expression for potential energy is

$$V_r = \tfrac{1}{2}k_r(r - r_0)^2 \tag{1}$$

where r_0 is the unstrained distance between two bonded atoms and k_r is bond stiffness. The relationship between restoration force and bond elongation can be derived as:

$$F_r = \frac{\mathrm{d}V_r}{\mathrm{d}r} = k_r(r - r_0) \tag{2}$$

An improved expression for potential energy is "Morse potential" [18,19], which can be written as:

$$V_r = D\left[\mathrm{e}^{-\alpha(r-r_0)} - 1\right]^2 \tag{3}$$

The relationship between bond elongation and restoration force can thus also be improved as:

$$F_r = \frac{\mathrm{d}V_r}{\mathrm{d}r} = \left\{-2\alpha D e^{-\alpha(r-r_0)}\left[\mathrm{e}^{-\alpha(r-r_0)} - 1\right]\right\} \tag{4}$$

Fig. 2 shows force-displacement curves derived from Morse potential energy. It is a non-linear curve. Bond

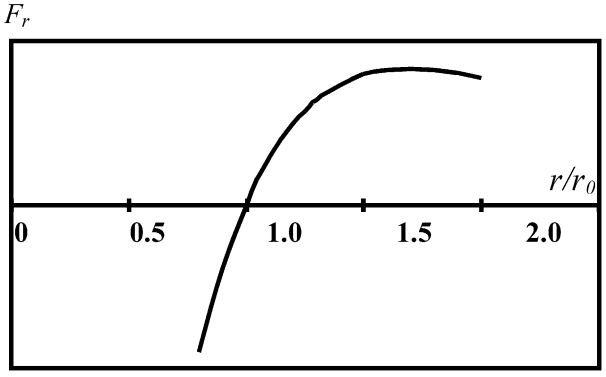

Fig. 2. Interactive force between bonded atoms based upon morse potential.

stiffness k_r is the slope of the curve, which can be derived by the derivative of the force with respect to bond length. The restoration force-bond elongation curve is approximately linear if bond elongation is small. Similar results can be achieved from both the harmonic potential energy and the Morse potential energy only if bond strain is small. As bond strain enlarges, the Morse potential energy becomes more accurate. The shape of Morse potential energy was not originally derived by quantum mechanics, but was later supported by quantum mechanics.

Harmonic potential energy is commonly taken in molecular mechanics to describe the angle bend interaction between two neighboring chemical bonds. It provides a linear relationship between restoration bending moment and bending angle. It is given as

$$V_\theta = \tfrac{1}{2}k_\theta(\theta-\theta_0)^2 \tag{5}$$

where θ_0 is the equilibrium bond angle. The relationship between bending moment and bending angle can be written as:

$$M_\theta = k_\theta(\theta-\theta_0) \tag{6}$$

2.3. Intermolecular interaction

Lennard–Jones' 6–12 function [20] is employed to describe the interaction between two atoms or monomers that are not chemically bonded. The potential energy of the Lennard–Jones function is expressed as:

$$V = 4\varepsilon\left[\left(\frac{\sigma}{r}\right)^{12}-\left(\frac{\sigma}{r}\right)^{6}\right] \tag{7}$$

where ε denotes the well depth and σ the zero-potential distance between two non-bonded atoms or monomers. The Lennard–Jones force (attraction or repulsion) between two non-bonded atoms can be written as:

$$F = \frac{4\varepsilon}{r}\left[-12\left(\frac{\sigma}{r}\right)^{12}+6\left(\frac{\sigma}{r}\right)^{6}\right] \tag{8}$$

2.4. Two-dimensional nano-scale finite element model for polymer fields

Two kinds of nano-scale elements are developed: the chemical bond element and the Lennard–Jones element.

2.4.1. Chemical bond element

A generic (united-atom) hydrocarbon polymer molecule is formed as shown in Fig. 3. Based upon the nature of the restoration force and moment, the covalent bond chain is modeled as a chain of elastic rods connected by elastic joints. Rods support the restoration force; elastic joints support restoration bending moments. The chain is divided (by dotted lines) into chemical bond elements. Each element is composed of

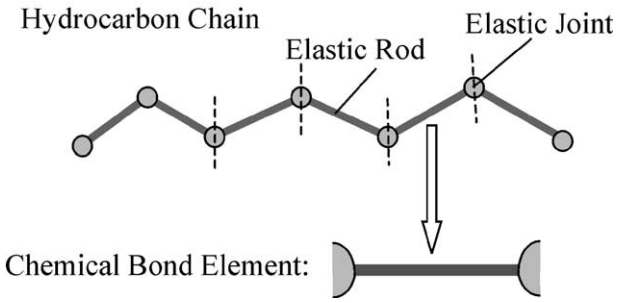

Fig. 3. Chemical bond element.

an elastic rod and two elastic joint halves, one on each of its two ends. The stretching stiffness of the chemical bond element is determined by the relationship between restoration force and bond elongation, which is determined either by Eq. (2) or (4). The bending stiffness of the elastic joint is equal to the bending stiffness of the covalent bond, which is determined by Eq. (6).

Chemical bond element nodal forces and displacements are shown in Fig. 4. There are three nodal forces for each node: F_{xi}, F_{yi}, M_i for node **i** and F_{xj}, F_{yj}, M_j for node **j**. There are three nodal displacements for each node: u_i, v_i, θ_ι for node **i** and u_j, v_j, θ_j for node **j**.

The nodal force increment and the displacement increment relationships in each loading step in the x-direction are:

$$\begin{aligned}\Delta F_{xi} &= k_r(\Delta u_i - \Delta u_j)\\ \Delta F_{xj} &= k_r(-\Delta u_i + \Delta u_j)\end{aligned} \tag{9}$$

where k_r is the stretching stiffness. If harmonic potential energy is used, k_r is the stretching stiffness defined in Eq. (2). If Morse potential energy is used, k_r is the slope of the restoration force vs. the bond elongation curve, which is shown in Fig. 2.

Assume the bending stiffness of joints **i** and **j** are $k_{\theta i}$ and $k_{\theta j}$, respectively, which are defined in Eq. (6). The bending stiffness of the half joint at node **i** equals "$2k_{\theta i}$" and the bending stiffness of the half joint at node **j** equals "$2k_{\theta j}$". Nodal bending moment increments induced in each loading step is expressed:

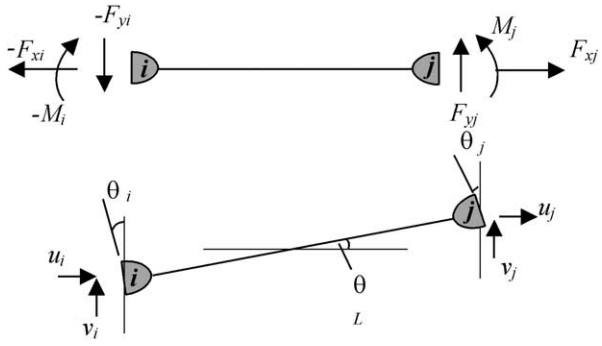

Fig. 4. Nodal forces and nodal displacements.

$$\begin{aligned}\Delta M_i &= -2\cdot k_{\theta i}\cdot(\Delta\theta_L - \Delta\theta_i)\\ \Delta M_j &= 2\cdot k_{\theta j}\cdot\left(\Delta\theta_j - \Delta\theta_L\right)\end{aligned} \tag{10}$$

where $\Delta\theta_L$ is further expressed as:

$$\Delta\theta_L = \frac{\Delta v_j - \Delta v_i}{L} \tag{11}$$

where L is the length of the element.

Based upon static equilibrium conditions, nodal force increments in the y-direction is derived:

$$\begin{aligned}\Delta F_{yi} &= \frac{\left(\Delta M_i + \Delta M_j\right)}{L}\\ \Delta F_{yj} &= -\frac{\left(\Delta M_i + \Delta M_j\right)}{L}\end{aligned} \tag{12}$$

Combining Eqs. (9)–(12), one derives nodal force and displacement increment relationships:

$$\begin{aligned}\Delta F_{xi} &= k_r\Delta u_i - k_r\Delta u_j\\ \Delta F_{yi} &= \frac{2\left(k_{\theta i}+k_{\theta j}\right)}{L^2}\Delta v_i + \frac{2k_{\theta i}}{L}\Delta\theta_i - \frac{2\left(k_{\theta i}+k_{\theta j}\right)}{L^2}\Delta v_j + \frac{2k_{\theta j}}{L}\Delta\theta_j\\ \Delta M_i &= \frac{2k_{\theta i}}{L}\Delta v_i + 2k_{\theta i}\Delta\theta_i - \frac{2k_{\theta i}}{L}\Delta v_j\\ \Delta F_{xj} &= -k_r\Delta u_i + k_r\Delta u_j\\ \Delta F_{yj} &= -\frac{2\left(k_{\theta i}+k_{\theta j}\right)}{L^2}\Delta v_i - \frac{2k_{\theta i}}{L}\Delta\theta_i + \frac{2\left(k_{\theta i}+k_{\theta j}\right)}{L^2}\Delta v_j - \frac{2k_{\theta j}}{L}\Delta\theta_j\\ \Delta M_j &= \frac{2k_{\theta j}}{L}\Delta v_i - \frac{2k_{\theta j}}{L}\Delta v_j + 2k_{\theta j}\Delta\theta_j\end{aligned} \tag{13}$$

The element stiffness matrix is written as:

$$[K]^e = \begin{bmatrix} k_r & 0 & 0 & -k_r & 0 & 0\\ 0 & \frac{2\left(k_{\theta i}+k_{\theta j}\right)}{L^2} & \frac{2k_{\theta i}}{L} & 0 & \frac{-\left(2k_{\theta i}+2k_{\theta j}\right)}{L^2} & \frac{2k_{\theta j}}{L}\\ 0 & \frac{2k_{\theta i}}{L} & 2k_{\theta i} & 0 & -\frac{2k_{\theta i}}{L} & 0\\ -k_r & 0 & 0 & k_r & 0 & 0\\ 0 & \frac{-2\left(k_{\theta i}+k_{\theta j}\right)}{L^2} & \frac{-2k_{\theta i}}{L} & 0 & \frac{2\left(k_{\theta i}+k_{\theta j}\right)}{L^2} & \frac{-2k_{\theta j}}{L}\\ 0 & \frac{2k_{\theta j}}{L} & 0 & 0 & \frac{-2k_{\theta j}}{L} & 2k_{\theta j}\end{bmatrix} \tag{14}$$

2.4.2. Lennard–Jones bond element

The Lennard–Jones bond is modeled as a non-linear spring element. Fig. 5 shows the Lennard–Jones force vs. the distance curve between two non-bonded atoms. If distance between them is smaller than 1.244 σ, the slope of the curve is positive; if distance between them is greater than 1.244 σ, the slope of the curve is negative. In order to reflect the actual nature of Lennard Jones bonds, the slope of the curve should define element stiffness. However, a negative element stiffness may induce the global stiffness matrix to not be positive definite. In order to overcome this difficulty, the following approach is adopted: If the slope of the force-distance curve is positive, the slope determines the stiffness of the element. If the slope is negative, the stiffness of the element is replaced by a small positive perturbation Δ rather than

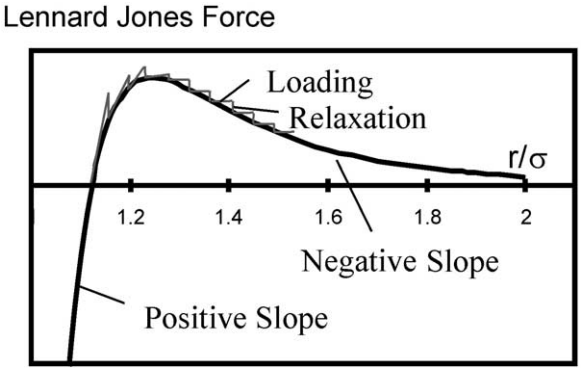

Fig. 5. Lennard–Jones force vs. inter-atomic distance.

the original negative value. Mathematically, the stiffness of the Lennard Jones element is defined as:

$$k_{l-j} = \begin{cases} \dfrac{\mathrm{d}F}{\mathrm{d}r} = \dfrac{4\varepsilon}{r^2}\left[156\left(\dfrac{\sigma}{r}\right)^{12} - 42\left(\dfrac{\sigma}{r}\right)^{6}\right] & \text{if } \dfrac{\mathrm{d}F}{\mathrm{d}r} > 0\\ \Delta & \text{if } \dfrac{\mathrm{d}F}{\mathrm{d}r} < 0\end{cases} \tag{15}$$

where "F" is the Lennard–Jones force between two non-bonded atoms, "r" is the distance between two non-bonded atoms and Δ is a small perturbation term employed to avoid the singularity of the stiffness matrix.

The replacement of the negative element stiffness with a small perturbation term might create error in the numerical calculation. In order to correct error caused by this replacement, a relaxation process follows each loading step as shown in Fig. 5. Details of the relaxation process will be introduced later in this section.

From Fig. 5, one can see that Lennard–Jones interactions decrease rapidly as distance increases in the negative slope region. Force becomes negligible if distance r is much greater than zero-potential distance σ. The cut-off distance in the example presented in this paper is 2.5 σ.

During the numerical process, distances between non-bonded atoms are examined at each loading step. If the distance between them is shorter than the cut-off distance (2.5 σ) of the Lennard–Jones force, a Lennard–Jones element is formed and inserted between them. Throughout polymer deformation, failed Lennard–Jones elements ($r > 2.5\ \sigma$) are removed from the system and newly formed Lennard–Jones elements ($r < 2.5\ \sigma$) are inserted until the polymer field finally fails.

2.5. Loading-relaxation processes

The global stiffness matrix is assembled using a method similar to a finite element approach.

The chemical bond element is a nonlinear element if Morse potential energy is adopted. The Lennard–Jones element is highly non-linear. In addition, a small perturbation term is used to replace the actual force-displacement relationship of the Lennard–Jones

bond when the force-distance slope is negative. This replacement violates the original nature of the Lennard–Jones bond. These three factors induce error in the numerical calculation.

In order to correct the error, a loading-relaxation process is adopted. Assume nodal positions and nodal forces before the k-th loading step are $\{X_{k-1}\}$ and $\{F_{k-1}\}$. The k-th step loading force is $\{\Delta F_k\}$. Then, the k-th step nodal displacement increment $\{\Delta U_k\}$ is solved from the following process:

Step 1: Solve nodal displacement increment $\{\Delta U_k\}$ from the following equation:

$$[K]\{\Delta U_k\} = \{\Delta F_k\} \tag{16}$$

Step 2: Calculate nodal positions:

$$\{X_k\} = \{X_{k-1}\} + \{\Delta U_k\} \tag{17}$$

Step 3: Calculate actual loading forces $\{\Delta F'_k\}$. The incremental axial nodal force ($\Delta F'_{xi}$ and $\Delta F'_{kj}$) applied to a chemical bond element (refer to Fig. 4) is calculated from its force-elongation relationship. If harmonic potential energy is used, the nodal force is calculated from Eq. (2); if Morse potential energy is used, the nodal force is calculated from Eq. (4). Subtracting axial nodal force before the loading step from the nodal force after the loading step, one derives the incremental axial nodal force. The incremental nodal force in the perpendicular direction ($\Delta F'_{yi}$ and $\Delta F'_{yj}$) and the incremental moment ($\Delta F'_{mi}$ and $\Delta F'_{mj}$) is calculated from Eq. (13). The nodal force applied to the Lennard–Jones element is determined by Eq. (8). Subtracting the nodal force before the loading step from that after the loading step, one derives the actual incremental Lennard–Jones interaction. Then, these incremental nodal forces are assembled into a incremental global nodal force matrix $\{\Delta F'_k\}$

Step 4: Check error.

If $\|\{\Delta F_k\} - \{\Delta F'_k\}\| < \varepsilon$, $\{\Delta U_k\}$ is accepted and the loading step ends.

If $\|\{\Delta F_k\} - \{\Delta F'_k\}\| > \varepsilon$, $\{\Delta U_k\}$ is not accepted and a relaxation process is required. "ε" is a small number. It controls the accuracy of the numerical process.

Step 5: Relaxation process. Let $\{\delta F\} = \{\Delta F_k\} - \Delta\{F'_k\}$. Calculate $\{\delta F\}$ induced nodal displacement matrix $\{\delta U\}$. Add $\{\delta U\}$ to $\{\Delta U_k\}$.

Repeat the process from step 2 to step 5 until

$$\|\{\Delta F_k\} - \{\Delta F'_k\}\| < \varepsilon.$$

3. Nano-scale element analysis of polymer fields

The numerical procedure includes three steps: polymer field generation, nano-element model establishment and polymer field deformation simulation.

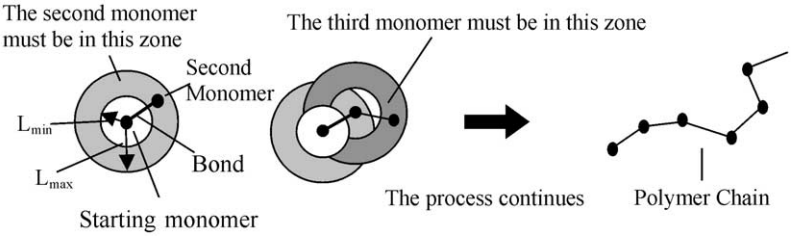

Fig. 6. Generation of the polymer chain.

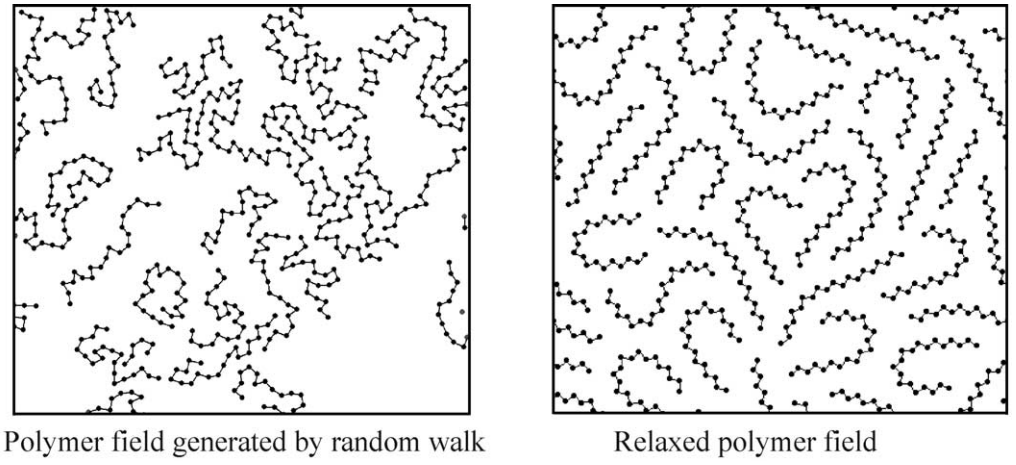

Fig. 7. Polymer field before force relaxation and after force relaxation.

3.1. Generation of the polymer field

A single idealized polymer chain is created by an off-lattice random walk, as shown in Fig. 6. The starting monomer is placed randomly inside the polymer field. Chemical bond lengths are restricted to a range between L_{min} and L_{max}, i.e., the second monomer must be located inside the shaded zone as shown in the left picture of Fig. 6. Bond angles are randomly selected. The third monomer is similarly generated. The process continues and a polymer chain is thus created.

A polymer field is generated through the following procedure: first, N starting monomers are distributed randomly within the material domain. Second, more monomers are added to the system, growing N polymer chains and generating a random polymer field. The random polymer field is not an actual polymer yet. It must be relaxed. Therefore, in the third step, the unbalanced force applied to each atom is calculated and a force relaxation process is then employed to relax the polymer field. Consequently, an equilibrium atomic field is generated. Fig. 7 illustrates polymer fields generated by this procedure. The picture on the left side is an unrelaxed polymer field produced by a random walk; the picture on the right side is a polymer field after force relaxation. Periodical boundary conditions are employed during both the random walk process and the relaxation process.

The next step is to examine the internal stress of the polymer field, which relates to monomer density. If the density were too high, a polymer field with a compressive pre-stress state would be created. If the density were too low, a polymer field with a tensile pre-stress state would be created.

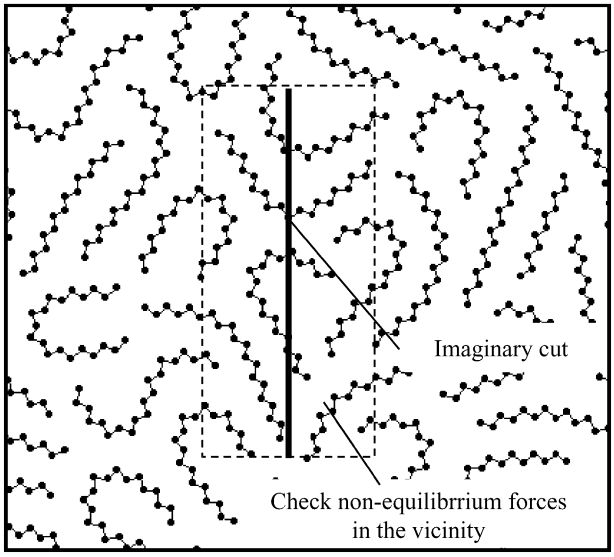

Fig. 8. Determine stress inside polymer field.

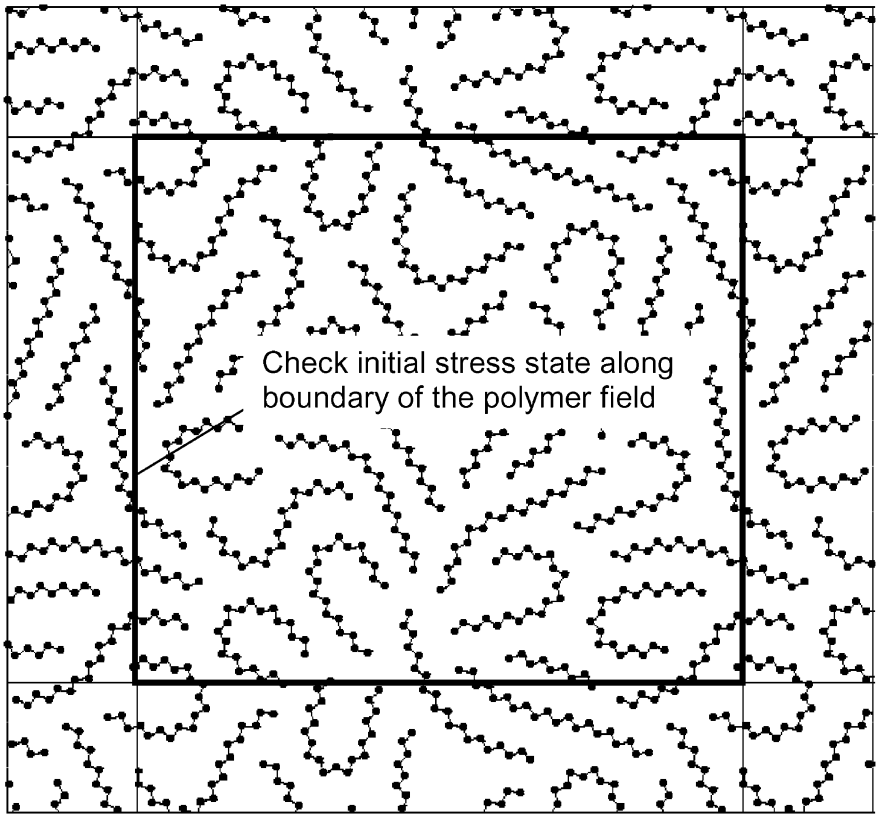

Fig. 9. Check stress along the boundary.

Refer to Fig. 8; the local stress of the polymer field is derived by the following procedure. An imaginary cut is made inside the polymer field. All chemical and Lennard–Jones bonds that connect the two sides of the imaginary cut are removed. Before the removal of these chemical and Lennard–Jones bonds, each atom is in an equilibrium position. This means the resultant force applied to each atom equals zero. After the removal of these chemical and Lennard–Jones bonds, monomers in the vicinity are no longer in an equilibrium state. In Fig. 8, the vicinity area is surrounded by a dotted rectangle. The rectangle is divided into two parts by the imaginary cut. The non-equilibrium force in each part is calculated. This represents interactions between monomers on both sides of the imaginary cut through the removed chemical and Lennard–Jones bonds. The resultant force of these interactions is translated into traction between both sides. As such, internal stress is derived.

In the examples presented in this paper, stress states along the boundaries of polymer field were examined. Referring to Fig. 9, the polymer field is marked by a dark boundary. Monomers outside the polymer field are generated in accordance with periodical boundary conditions. We made imaginary cuts along the four sides of the polymer field and examined traction on the boundary. Stresses were subsequently calculated. By adjusting polymer field density, the initial zero-stress state of the polymer field was obtained.

3.2. Nano-scale element model for the polymer field

Fig. 10 illustrates the finite element model. The polymer chain is modeled as a chemical bond chain. Lennard–Jones elements are represented by dotted lines. They connect nearby hydrocarbon monomers, including monomers on the same chain and on different chains, except those chemically bonded. During polymer deformation, failed Lennard–Jones bond elements are removed and new Lennard-Jones elements are inserted into the polymer field during each loading step. The parameters used are similar to those used by Chui and Boyce [11] as follows:

$$\begin{aligned} k_r &= 2.78\ \text{aJ/Å}^2\text{/bond} & r_o &= 1.47\text{Å} \\ k_\theta &= 0.498\ \text{aJ/Rad./bond} & \theta_o &= 1.88\text{Rad.} \\ \varepsilon &= 0.585 \times \left(10^{-3}\right)\ \text{aJ/bond} & \sigma &= 3.53\text{Å} \end{aligned} \tag{18}$$

Notations used in the above equations are the same as the notations used in Eqs. (1)–(8).

3.3. Stiffness and strength of the polymer field

Polymer field deformations under unidirectional loads are simulated. Two examples are presented here. Both polymer fields include 30 polymer chains. Each chain

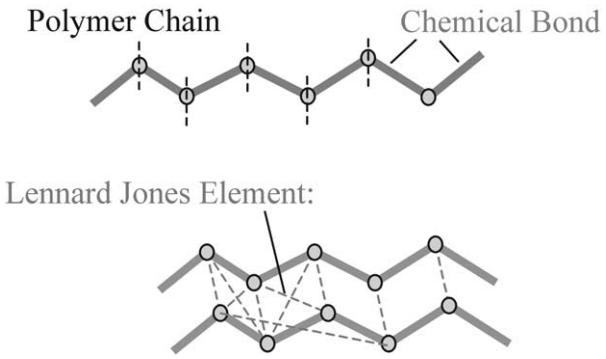

Fig. 10. Nano-scale element model for polymer field.

Table 1
Sizes of polymer fields

Example No.	Number of monomers	Width of polymer field	Height of polymer field
1	588	71	64
2	573	63	57

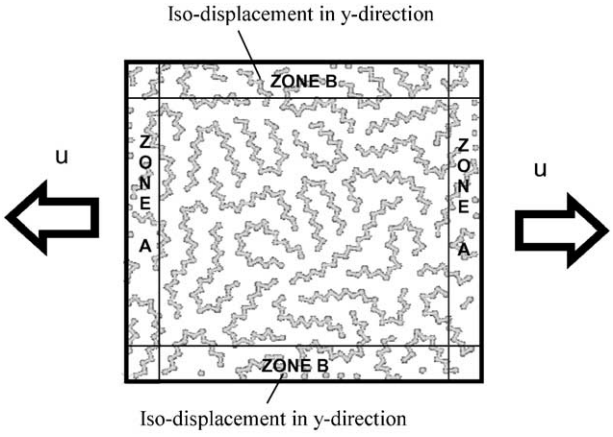

Fig. 11. Boundary conditions in the numerical calculation.

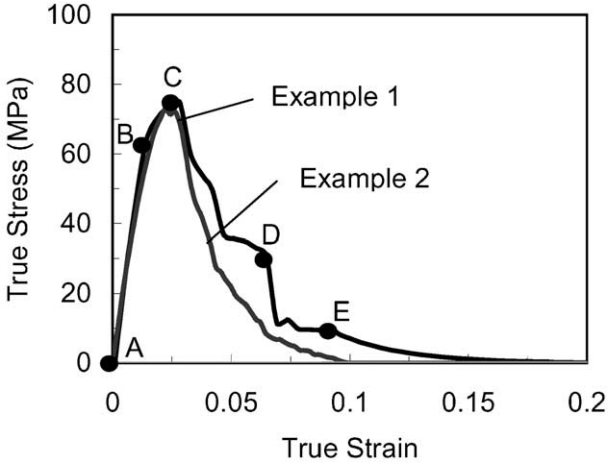

Fig. 12. True stress–true strain curve.

has approximately 20 monomers. The number of monomers in each polymer field and the size of each polymer field are listed in Table 1.

The boundary conditions, shown in Fig. 11, are similar to boundary conditions used in continuum mechanics. In the x-direction, there are two end zones, defined as zones "A". x-Direction displacements of all monomers in each zone "A" are coupled. They are forced to move an equal distance during each loading step. Looking at Fig. 11, monomers in zone "A" on the right side of the field would move toward the right and monomers on the left side of the field would move toward the left. During each step, an elongation of 0.31 Å is applied. Totally 50 loading steps are applied to the polymer field.

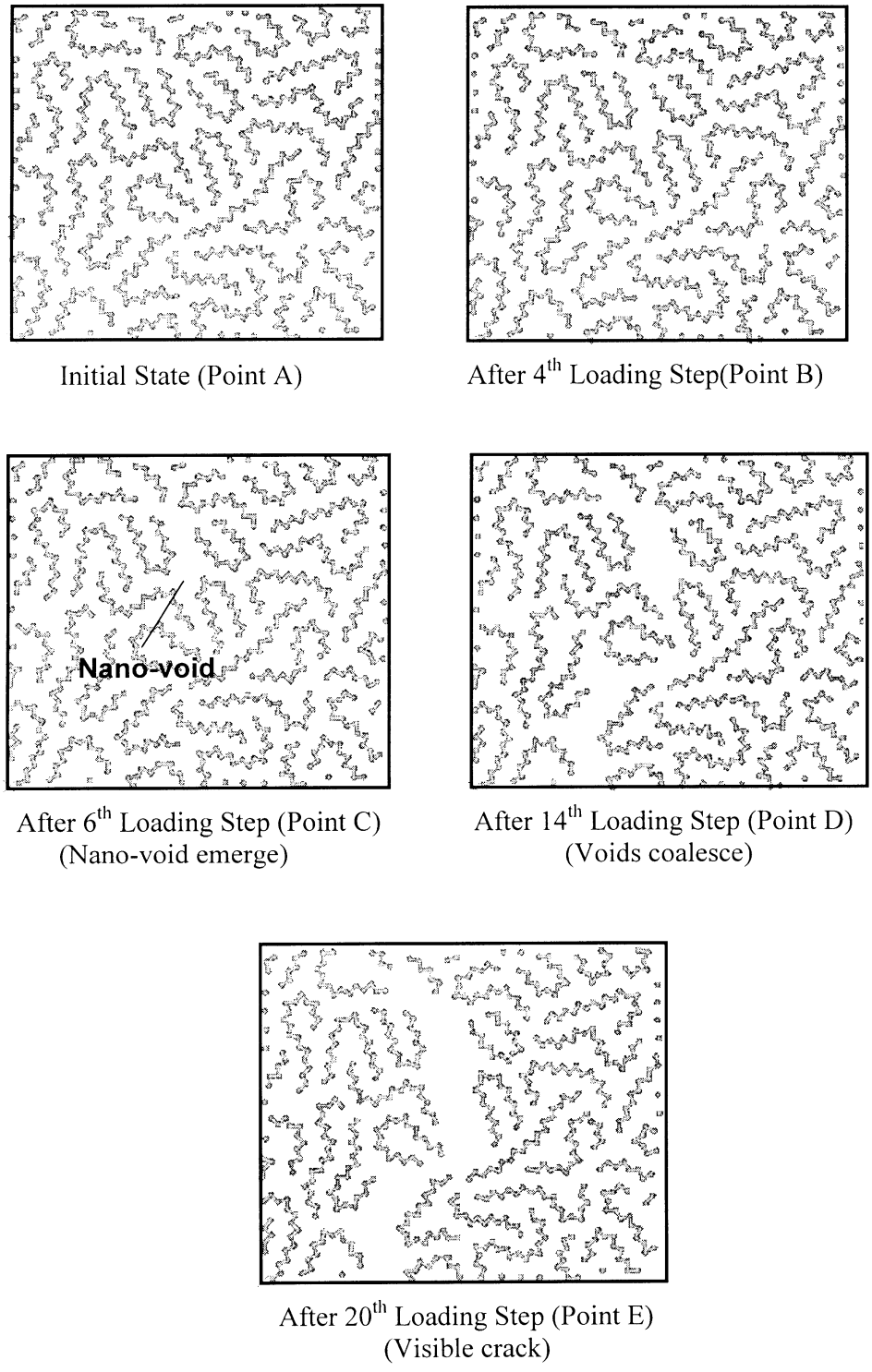

Fig. 13. Step by step polymer field deformation.

In the y-direction, there is an upper and a lower boundary zone, defined as zones "B". In order to prevent an edge effect, an iso-displacement condition in the y-direction is applied to monomers in each "B" zone, i.e., y-direction displacements for all monomers in each zone "B" are coupled into one degree of freedom.

Fig. 12 presents true-stress and true-strain curves for the two polymer fields. Stress is calculated based upon the assumption that polymer field thickness equals the unstrained Lennard–Jones bond length. The stress–strain curve is linear in the small strain regime. The initial slopes of both curves almost coincide. The initial moduli for these two polymer fields are 4.91 and 4.74 GPa, respectively. The slopes subsequently decrease. The strengths of the two polymer fields (the maximum values of the stress) are 74.7 and 72.8 MPa, respectively. Both polymer fields fail when strain approximates 3%.

After each loading step, polymer field conformation is examined in order to explain the failure mechanism. Fig. 13 shows polymer field conformation for the first example at critical points corresponding to the stress-strain curve shown in Fig. 12: specifically, points A, B, C, D and E. After the 6th loading step, namely point C, nanoscale-voids begin to develop. After the 14th loading step, namely point D, several voids coalesce. After the 20th loading step, namely point E, a crack becomes visible. The polymer field fractures along the crack.

The deformation process and failure mechanism could be understood as follows. At low strains, where monomers are in the vicinity of their unstrained positions, both chemical and Lennard–Jones bonds exhibit approximate linear force–displacement relationships. Thus, the whole polymer field would be an approximate linear system. This would explain the initial linear stress–strain relationship. With an increase in strain, distances between polymer chains increase and Lennard–Jones attractions decrease. Thus polymer stiffness decreases. With a continuing decrease in Lennard–Jones attractions, the polymer field becomes less uniform and voids emerge. The structure weakens and ultimately the polymer field fails.

Although no comparison to experiment is possible for this simplified 2-D polymer field, the potential of the method to simulate nano-scale deformation has been demonstrated.

4. Concluding remarks

A nano-scale element approach is developed in this paper. Two types of two-dimensional nano-scale elements are formulated: the chemical bond element and the Lennard-Jones bond element. The deformation of a simplified 2-D polymer field is simulated in order to generate a macro-level stress-strain curve based upon inter-atomic and inter-molecular force fields. When the deformation of the polymer field is examined step-by-step, nano-scale void generation, void coalescence and crack formation are observed. Direct visualization of the deformation process enables an understanding of the failure mechanism.

An actual polymer field has a three-dimensional conformation. It is impossible to model polymer chain interlocks and entanglements inside a three-dimensional polymer field using a two-dimensional model. In order to quantitatively analyze the stiffness, strength, and failure mechanism of the polymer field, a three-dimensional nano-scale element model is required. This is currently under development.

Polymer field initial states are relaxed using a force relaxation method. Thus, all monomers are in their equilibrium positions at the initial state. This would correspond to the zero-stress state of the polymer field at low temperature. If the temperature were increased, thermal motion would occur, and monomers would deviate from their equilibrium positions. As a consequence, polymer modulus and strength might decrease as temperature increases. By assigning potential energy to each monomer directly inside an equilibrium polymer field, one might be able to analyze the influence of temperature on the modulus and strength of the polymer field using quasi-static analysis. This will be explored in the future.

The numerical approach developed in this paper would be valuable not only for polymer fields, but also for the nano-scale analysis of other materials.

References

[1] Berendsen HJC, Postma JPM, van Gunsteren WF, DiNola A, Haak JR. Molecular dynamics with coupling to an external bath. Journal of Chemical Physics 1984;81:3684.
[2] Brown D, Clarke JHR. Molecular dynamics simulation of an amorphous polymer under tension. 1. Phenomenology. Macromolecules 1991;24:2075.
[3] McKechnie JI, Haward RN, Brown D, Clarke JHR. Effects of chain configurational properties on the stress–strain behavior of glassy linear polymers. Macromolecules 1993;26:198.
[4] Lu JP. Elastic properties of carbon nanotubes and nanoropes. Physical Review Letters 1997;79:1297.
[5] Srivastava D, Menon M, Cho K. Nanoplasticity of single-wall carbon nanotubes under uniaxial compression. Physical Review Letters 1999;83(15).
[6] Ozaki T, Iwasa Y, Mitani T. Stiffness of single-walled carbon nanotubes under large strain. Physical Review Letters 2000;84:1712.
[7] Yao N, Lordi V. Young's modulus of single-walled carbon nanotubes. Journal of Applied Physics 1998;84:1939.
[8] Frankland SJV, Brenner DW. Molecular dynamics simulations of polymer-nanotube composites. Materials Research Society Symposium Proceedings 1999:593.
[9] Frankland SJV, Caglar A, Brenner DW, Griebel M. Reinforcement mechanism in polymer nanotube composites: simulated non-bonded and cross-linked system. Materials Research Society Symposium Proceedings 2000:594.

[10] Parrinello M, Rahman AJ. Strain fluctuations and elastic constants. Journal of Chemical Physics 1982;76:2662.
[11] Chui C, Boyce MC. Monte Carlo modeling of amorphous polymer deformation: evolution of stress with strain. Macromolecules 1999;32:3795.
[12] Boyce MC, Socrate S, Llana PG. Constitutive model for the finite deformation stress-strain behavior of poly(ethylene terephthalate) above the glass transition. Polymer 2000;41:2183.
[13] Theodorou DN, Suter UW. Atomistic modeling of mechanical properties of polymeric glasses. Macromolecules 1986;19:139.
[14] Rappe AK, Casewit CJ. Molecular mechanics across chemistry. Sausalito, California: University Science Books; 1997.
[15] Bjerrum N. Uber die Ultraroten Spektren der Gase. III. Die Konfiguration des Kohlendioxydmolekuls und de Gestze der Intramolekularen Krafte. Verhandle Deut Physik Ges 1919;16:737.
[16] Hill TL. On steric effects. Journal of Chemical Physics 1946;16:399.
[17] Westheimer FH, Mayer JE. The theory of the racemization of optically active derivatives of diphenyl. Journal of Chemical Physics 1946;14:733.
[18] Morse PM. Diatomic molecules according to the wave mechanics. II. Vibrational level. Physical Review 1929;34:57.
[19] Dostrovsky I, Hughes ED, Ingold CK. Mechanism of substitution at a saturated carbon atom. Part XXXII. The role of steric hindrance (Section G) magnitude of steric effects, range of occurrence of steric and polar effects, and place of the Wagner rearrangement in nucleophilic substitution and elimination. Journal of Chemical Society 1946;173.
[20] Lennard Jones LE. On the determination of molecular fields—II. From the equation of state of a gas. Proc R Soc London, Ser A 1924;106:463.